Research Article

Received: 18 November 2008 Revised: 8 July 2009 Accepted: 21 September 2009 Published online in Wiley Interscience: 25 January 2010

(www.interscience.wiley.com) DOI 10.1002/pi.2769

Tensile creep behaviour of polymethylpentene–silica nanocomposites

Andrea Dorigato* and Alessandro Pegoretti

Abstract

For the first time, poly(4-methyl-1-pentene) (PMP) nanocomposites were prepared by melt compounding 2 vol% of fumed silica nanoparticles, in order to study the role of the nanofiller surface area and functionalization on the tensile mechanical response of the material, with particular focus on its creep behaviour. The high optical transparency of the polymer matrix was substantially preserved in the nanocomposites, while the mechanical properties (in particular the creep stability) were improved. Dynamic mechanical thermal analysis showed an improvement of the storage modulus, more evident above the glass transition temperature of the polymer matrix. Uniaxial tensile tests evidenced that the elastic modulus of the material was positively affected by the presence of silica nanoparticles, even if a slight reduction of the strain at break was detected. The reduction of the tensile creep compliance was proportional to the surface area of the nanofiller, being more evident at high stresses and elevated temperatures. Findley's law furnished a satisfactory fitting of the creep behaviour of the composites, even at high temperatures. It clearly emerges that the incorporation of fumed silica nanoparticles in PMP can be an effective way to overcome the problem of the poor creep stability of polyolefins, especially at high temperatures and high stresses. Moreover the possibility of retaining the original transparency of the material is fundamental for the production of completely transparent PMP components.

Keywords: polymethylpentene; nanocomposites; creep; transparency

INTRODUCTION

Inorganic nanoparticles have been often added to polymeric matrices to improve their toughness and strength, to increase their thermal stability and to enhance the barrier properties of the pristine polymer.[1–4] Thermoplastic polymers make up the major part of world plastic consumption, because of their low density, good processability and low cost. However, in some applications their use is limited by several drawbacks, including poor creep stability, especially under long-lasting stresses. Reinforcing with small amounts of nanoparticles has proven to be an effective solution to enhance the creep resistance of thermoplastics. For example, titania nanoparticles were used to markedly reduce the creep compliance of nylon-66,[5–8] while addition of alumina nanoparticles resulted in an enhancement of the creep stability of polystyrene.[9] Also reported was a marked reduction of the creep compliance of high-density polyethylene (HDPE) filled with submicrometre titania particles,[4] acicular titania nanoparticles[10] and organoclays.[11] A commonly accepted explanation for the stiffening effect of inorganic nanoparticles is that they can effectively restrict the motion of polymer chains, influencing the stress transfer at the nanoscale, with positive effects on the final creep stability of the material.

Poly(4-methyl-1-pentene) (PMP) is a semi-crystalline polyolefin currently used for automotive components, light covers, pacemaker parts, and blood collection, medical and laboratory devices.[1,2] This polymer possesses a unique combination of remarkably low density (0.83 g cm^{-3}), relatively high thermal stability (melting peak at 230 °C), chemical resistance and optical transparency (more than 90% in the range of visible light). In the scientific literature very few articles regarding the preparation and the characterization of PMP nanocomposites are to be found. For example, Wanjale and Jog studied the effect of an organic compatibilizer on the thermomechanical properties of PMP–clay nanocomposites, finding a delay in the degradation process, an increase in the storage modulus and a better dimensional stability with respect of the unfilled material.[1,2] Hadal *et al*. described the surface deformation behaviour and susceptibility to surface damage of clay-reinforced PMP nanocomposites.[3]

As recently reported, fumed silica nanoparticles can substantially improve the stiffness and toughness of polyolefins, such as linear low-density polyethylene[12] prepared using both metallocene and Ziegler–Natta catalysts, with a strong dependence on the surface area of the nanofillers. Therefore, the objective of the work reported in the present paper was to assess the contribution of silica nanoparticles to the mechanical response of PMP, with particular focus on its tensile creep behaviour.

EXPERIMENTAL

Sample preparation

The PMP matrix utilized in this work was TPX RT18, supplied by Mitsui Chemicals America, with a density of 0.833 g cm^{-3} and a melt flow rate at 190 °C and 2.16 kg of 26 g (10 min)$^{-1}$.

* *Correspondence to: Andrea Dorigato, University of Trento, Department of Materials Engineering and Industrial Technologies, via Mesiano 77, 38100 Trento, Italy. E-mail: andrea.dorigato@ing.unitn.it*

University of Trento, Department of Materials Engineering and Industrial Technologies, via Mesiano 77, 38100 Trento, Italy

Table 1. Density and specific surface area values of the fumed silica nanofillers utilized in this work, with estimation of the primary nanoparticle size

Sample	Density[a] (g cm^{-3})	BET surface area[b] (m^2 g^{-1})	Estimated primary nanoparticle size (nm)
A90	2.50 ± 0.01	99.5 ± 0.7	24.1
A200	2.27 ± 0.02	196.6 ± 1.7	13.4
Ar816	2.04 ± 0.01	159.2 ± 1.3	18.5
A380	2.41 ± 0.02	320.8 ± 3.4	7.8

[a] Measured using a Micromeritics Accupyc 1330 helium pycnometer.
[b] Measured using an ASAP 2010 accelerated surface area and porosimetry machine.

Various Aerosil fumed silicas, supplied by Degussa, were used as nanofillers. Table 1 summarizes the most important properties of these nanoparticles. Densities were measured using a Micromeritics Accupyc 1330 helium pycnometer, while specific surface area values were determined using an ASAP 2010 accelerated surface area and porosimetry machine, following the Brunauer–Emett–Teller (BET) procedure. From these data it was possible to calculate the mean diameter of fumed silica primary nanoparticles, according to

$$d = \frac{6000}{\rho \times \mathrm{SSA}} \tag{1}$$

where ρ is the filler density, expressed in g cm^{-3}, and SSA is the specific surface area in m^2 g^{-1}. As is evident from Table 1, the nanoparticles were different in terms of surface area. Silica nanoparticles surface treated with exadecylsilane (Aerosil r816) and having a surface area of about 160 m^2 g^{-1} were also used.

PMP–silica nanocomposites were prepared by a melt-compounding process, using a Haake PolyLab system consisting of a Rheomix 600 internal mixer and a Rheocord 300p control module for continuous monitoring of torque, motor speed and temperature. Both pure PMP and nanocomposites filled with 2 vol% of the various fumed silicas were melt-mixed for 5 min at a temperature of 240 °C and a rotor speed of 50 rpm. Square sheets were then obtained by compression moulding for 10 min at 240 °C in a Carver laboratory press under an applied pressure of 0.2 kPa. Unfilled material is denoted as PMP, while the nanocomposites are designated as PMP followed by a number representing the surface area or surface treatment of the adopted nanofiller (e.g. PMP90 refers to a sample filled with 2 vol% of Aerosil 90).

Optical properties

Thin (150 μm) specimens for evaluation of optical properties were prepared by pressing a small portion of the pure PMP and nanocomposite sheets under two glass slides at 240 °C for 5 min. The transparency of the samples was evaluated using a Jasco V570 spectrophotometer, in a wavelength interval between 200 and 800 nm and at a scan speed of 200 nm min^{-1}. The transmittance (T) as a function of the wavelength (λ) was determined. Photographs of the same samples were also obtained using a Nikon Coolpix 4500 photocamera.

Mechanical properties

Dynamic mechanical thermal analysis tests were conducted using a MKII Polymer Laboratories dynamic mechanical thermal analyser, at a heating rate of 3 °C min^{-1} and a frequency of 1 Hz, under tensile configuration.

Quasi-static and creep tensile mechanical tests were performed with an Instron model 4502 universal testing machine. For the evaluation of the elastic modulus, ISO 527-1BA samples were tested at a crosshead speed of 0.25 mm min^{-1}. The displacement was determined using an Instron model 2620 clip-on extensometer, with a gauge length of 12.5 mm. Tensile tests at break were performed using ISO 527-1BA samples at a crosshead speed of 10 mm min^{-1}. In this case, due to the large displacement involved, the deformation of the specimen was derived from the crosshead displacement. At least five specimens were tested for each sample.

Creep tests were performed on rectangular samples 100 mm long, 5 mm wide and 0.6 mm thick. Isothermal creep tests were conducted for 1 h in a thermostatic chamber at a temperature of 30 °C, under a constant stress of 3 MPa. Isothermal creep tests at various stresses were conducted for 1 h at a temperature of 30 °C on pure PMP and PMP380 samples. Six different stress levels were chosen, i.e. 3, 4.5, 6, 9, 10.5 and 12 MPa. Creep compliance curves at various stresses and stress–strain isochronous curves were constructed for various creep times. Creep tests at six temperatures, ranging from 30 to 88 °C, were performed for 1 h on PMP and PMP380 samples, at a constant stress of 3 MPa.

Creep modelling

Strain in isothermal tensile creep, $\varepsilon(t,\sigma)$, depends on time t and stress σ, and it is usually considered as consisting of three components:[13–17] (i) elastic (instantaneous, reversible) $\varepsilon_e(\sigma)$; (ii) viscoelastic (time-dependent, reversible) $\varepsilon_{ve}(t,\sigma)$; and (iii) plastic (time-dependent, irreversible) $\varepsilon_p(t,\sigma)$:

$$\varepsilon(t,\sigma) = \varepsilon_e(\sigma) + \varepsilon_{ve}(t,\sigma) + \varepsilon_p(t,\sigma) \tag{2}$$

Linear stress–strain behaviour implies that the magnitude of the three components is linearly proportional to the applied stress, so that creep compliance $D(t)$, defined as the ratio between the total creep strain $\varepsilon(t,\sigma)$ and the applied stress, is a function of time only. If no plastic deformation is produced in the course of the creep test, the tensile compliance for the isothermal creep can be expressed as follows:

$$D(t) = D_e + D_{ve}(t) \tag{3}$$

In the present work, Eqn (3) was adopted to analyse the experimental data. In fact, all the experiments were performed under the same applied stress in order to avoid nonlinearity effects. Moreover, the specimens recovered their initial length after unloading, thus excluding the presence of plastic deformation.

A time–temperature superposition principle was adopted to analyse the creep behaviour, on the basis of the following equation:[18]

$$D(\log t + \log a_{T_0}, T) = D(\log(t a_{T_0}), T) = D(\log t, T_0) \tag{4}$$

where a_{T_0} is the time shift factor necessary to superpose the isotherm at temperature T on the reference creep curve at temperature T_0. Master curves at a reference temperature T_0 and a reference stress σ_0 were hence obtained, describing the creep response over a wide time scale.

The ability to model the viscoelastic creep response allows a better understanding of the underlying deformation mechanisms and

provides a design tool for long-term load-bearing applications.[19] In the present paper, Findley's model was adopted to fit experimental data. This model can be obtained by expanding the Kohlrausch–Williams–Watts (KWW) model, generally described by a Weibull-like function,[20–23] as a series and ignoring all but the first term:[24,25]

$$D(t) = D_0 + k(t)^n \quad (5)$$

where D_0 is the elastic instantaneous creep compliance, k is a coefficient related to the magnitude of the underlying retardation process and n is an exponent tuning the time dependency of the creep process. D_0 and k are functions of environmental variables, including temperature, moisture, etc.[26]

In this work, creep curves at different temperatures for PMP and PMP380 samples were fitted using Findley's model, in order to investigate possible correlations between the viscoelastic response of the material and the fitting parameters.

RESULTS AND DISCUSSION

Optical properties

Transmittance (T) curves of pure PMP and silica-filled nanocomposites in the visible wavelength range are shown in Fig. 1, while photographs of the samples are shown in Fig. 2. It is evident that the transparency is not much influenced by the presence of the nanoparticles. In all cases the transmittance is around 85–90% for wavelengths in the visible region (i.e. above 400 nm), while for shorter wavelengths the transparency of the nanocomposites is markedly reduced with respect to the pure PMP matrix. Similar behaviour has already been reported by Ou and Hsu for COC–silica nanocomposites.[27,28] Considering the packaging applications of PMP, the enhancement of the absorption coefficient at short wavelengths (i.e. below 400 nm) induced by the nanoparticles can certainly be considered as a positive effect, since the material barrier properties towards UV radiation are enhanced. On the other hand, the good optical properties of PMP in the visible region are preserved after the addition of silica nanoparticles.

Dynamic mechanical behaviour

Relative storage modulus of fumed silica-filled samples is shown in Fig. 3 for various temperatures from −20 up to 150 °C. A general consideration is that the introduction of small amounts of silica nanoparticles leads to an appreciable enhancement of the storage modulus E'. The stiffening effect is more enhanced above the glass transition temperature of the host matrix (around 40 °C), when the chain mobility is higher and the chain blocking mechanism due to the nanoparticles is more effective. Moreover, above room temperature the increase of E' values is higher as the surface area of the nanofiller increases, while the presence of a surface treatment does not appreciably affect the dynamic mechanical behaviour of the material.

Quasi-static tensile tests

Representative stress–strain curves obtained from quasi-static tensile mechanical tests are shown in Fig. 4, while the results are summarized in Table 2. The elastic modulus slightly increases when the nanoparticles are added, this improvement being more evident as the nanofiller surface area increases. In fact, even if elastic modulus of the low-surface-area fumed silica-filled sample (PMP90) is practically coincident with that of pure PMP, the introduction of silica nanofillers at higher surface area leads to

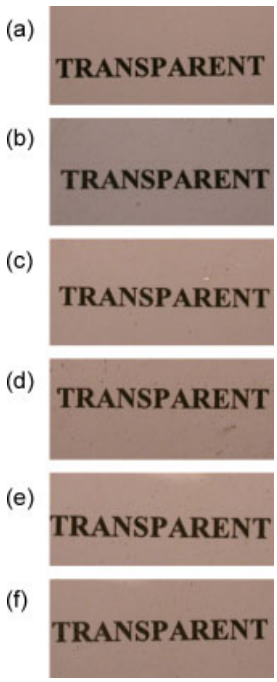

Figure 2. Optical transparency of PMP and nanocomposites: (a) uncovered text, and text covered by (b) PMP, (c) PMP90, (d) PMP200, (e) PMP380 and (f) PMPr816.

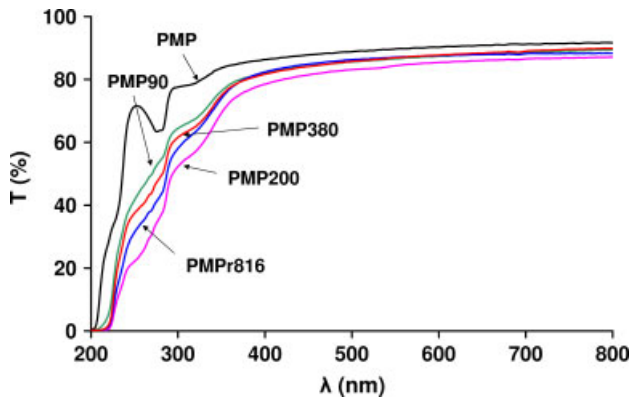

Figure 1. Transmittance values as a function of the wavelength for PMP and nanocomposites.

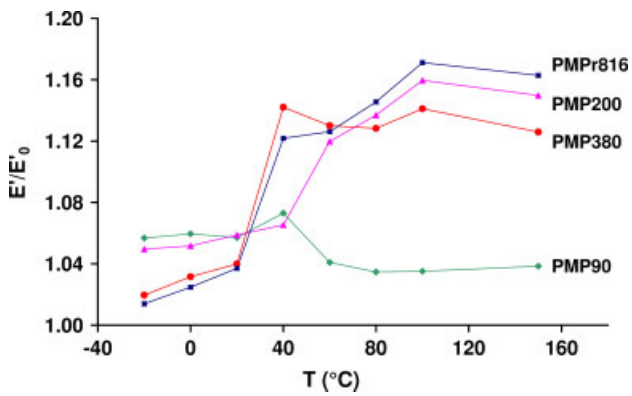

Figure 3. Relative storage modulus of PMP–silica nanocomposites.

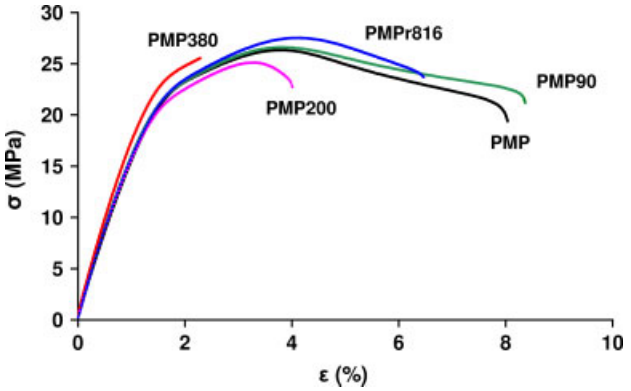

Figure 4. Quasi-static tensile test results of PMP and nanocomposites.

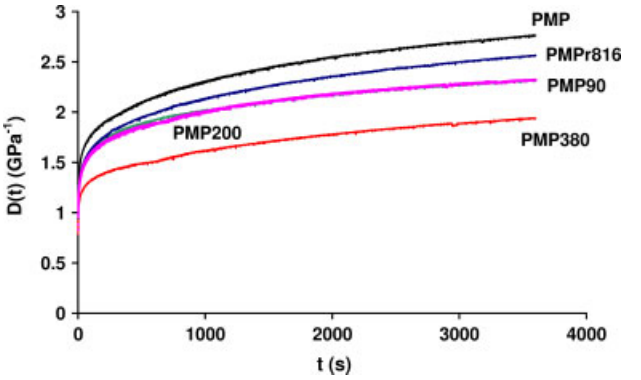

Figure 5. Creep compliance curves of PMP and nanocomposites ($T = 30\,^{\circ}C$, $\sigma = 3$ MPa).

Table 2. Quasi-static tensile mechanical properties of PMP and nanocomposites

Sample	E (MPa)	σ_y (MPa)	ε_y (%)	σ_r (MPa)	ε_r (%)
PMP	1.36 ± 0.07	26.6 ± 0.6	3.7 ± 0.1	20.7 ± 1.1	7.8 ± 1.1
PMP90	1.31 ± 0.08	27.3 ± 0.4	3.9 ± 0.1	21.5 ± 1.1	8.6 ± 1.6
PMP200	1.47 ± 0.07	25.9 ± 0.8	3.2 ± 0.3	22.9 ± 1.2	4.1 ± 1.0
PMPr816	1.48 ± 0.09	27.5 ± 0.1	3.2 ± 0.2	24.9 ± 1.7	6.2 ± 1.0
PMP380	1.58 ± 0.04	24.7 ± 1.7	2.2 ± 0.8	24.7 ± 1.7	2.2 ± 0.9

Table 3. Creep compliance components of PMP and nanocomposites ($T = 30\,^{\circ}C$, $\sigma = 3$ MPa)

Sample	D_e (GPa^{-1})	D_{ve2000} (GPa^{-1})	D_{t2000} (GPa^{-1})
PMP	1.07	1.48	2.55
PMP90	1.02	1.16	2.18
PMP200	1.07	1.09	2.17
PMPr816	1.08	1.27	2.36
PMP380	0.92	0.86	1.78

an increase of the stiffness of 8% for PMP200 and of 16% for PMP380. This result can be explained considering that the extent of the interphase considerably increases with the surface area of the nanofiller; consequently the stress-transfer mechanism is favoured when a wide interface is available.

As previously reported for dynamic mechanical properties, the elastic modulus is not affected by the surface functionalization of the nanoparticles. The stress at yield of nanocomposites is practically the same as that of pure PMP matrix, while a certain embrittlement, with a reduction of the deformation at break, can be observed for filled samples. The reduction of the material strain at break is also proportional to the surface area of the silica nanoparticles. Even in this case, strain at break of the PMP90 nanocomposite is similar to that of the unfilled matrix, while the embrittlement begins to be evident for PMP200, in agreement with the higher chain blocking effect expected as the filler surface area increases. Nevertheless, it is worth noting that for PMPr816 nanocomposites the strain at break is similar to that of pure PMP sample, thus indicating that an appropriate surface functionalization can preserve material ductility. This result can be tentatively explained considering that the organosilane on the surface of the nanofiller may act as a compatibilizing agent, creating an efficient interphase and improving the stress-transfer mechanism between matrix and filler.

Creep behaviour

Isothermal creep compliance curves of PMP and PMP–silica nanocomposites, at a reference temperature of 30 °C and applied stress of 3 MPa, are shown in Fig. 5, while the values of the instantaneous creep compliance (D_e), of the viscoelastic component after 2000 s (D_{ve2000}) and of the total creep compliance after 2000 s (D_{t2000}) are reported in Table 3. A marked reduction of the creep compliance is observed for silica-filled samples, especially for samples filled with silica particles with the highest surface area. This improvement in the creep stability is due to a substantial reduction both of the elastic and of the viscoelastic component of the total creep compliance. The enhancement of the creep resistance due to the introduction of nanoparticles has already been reported by others researchers, such as Zhang and co-workers for PA66–TiO_2 nanocomposites,[2,29] Ranade *et al.*[30] and Pegoretti and co-workers for HDPE–clay nanocomposites[11] and HDPE–titania nanocomposites.[10] The reduction of the chain mobility due to the presence of the silica nanoparticles can provide an effective explanation for the enhancement of material stability under creep conditions. As previously observed for HDPE filled with spherical or acicular titania nanoparticles,[4] the presence of a surface functionalization on the particles worsened the creep behaviour of the resulting nanocomposites. This behaviour can be related to the presence of a interfacial region, surrounding the treated particles, more compliant than the bulk polymer matrix.

Isothermal creep curves at 30 °C and various stress levels are shown in Fig. 6 for PMP and PMP380 samples, while Fig. 7 shows isochronous stress–strain curves. The positive effect of the silica nanoparticles in reducing the creep compliance of the material is particularly evident as the stress level increases. In fact at 12 MPa, the unfilled sample has a higher creep compliance, with tertiary creep and final yielding, while the PMP380 nanocomposite remains in the secondary creep region over the entire testing time. This means that the chain blocking mechanism of silica nanoparticles is more effective as the stress level increases and the mobility of polymeric chains is accelerated by the presence of strain-induced free volume.[31] The positive effect of the silica nanoparticles on the creep resistance of PMP is also evident, considering the isochronous curves shown in Fig. 7. It is clear that the deformational behaviour of pure PMP at 600 s is practically the same as that of PMP380 at 3600 s. These considerations

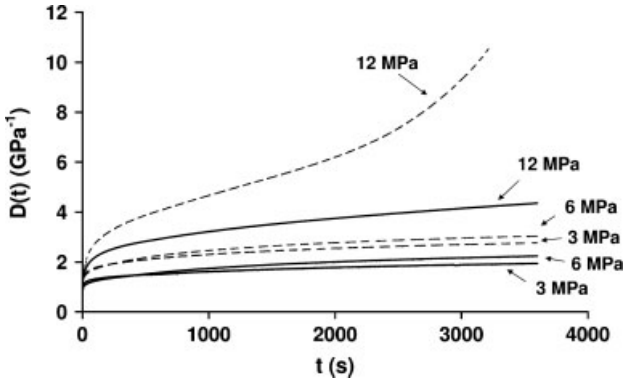

Figure 6. Isothermal creep compliance curves of PMP (dashed curves) and PMP380 nanocomposite (solid curves) at various stress levels ($T = 30\,^{\circ}$C).

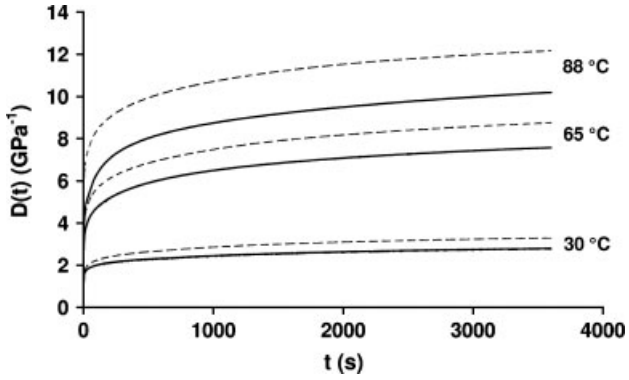

Figure 8. Creep compliance curves of PMP (dashed curves) and PMP380 nanocomposite (solid curves) at various temperatures ($\sigma = 3$ MPa).

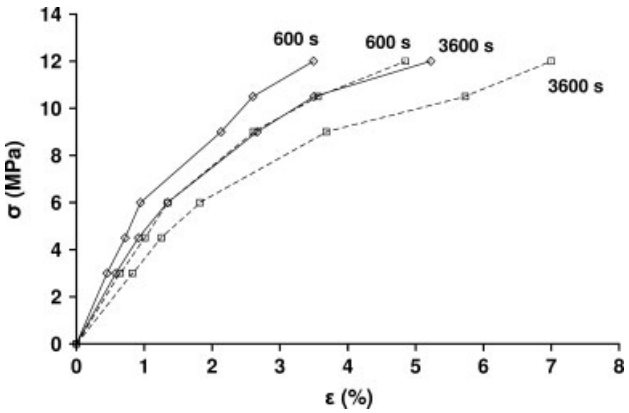

Figure 7. Isochronous stress–strain curves of PMP (dashed curves) and PMP380 nanocomposite (solid curves) at 600 s and at 3600 s ($T = 30\,^{\circ}$C).

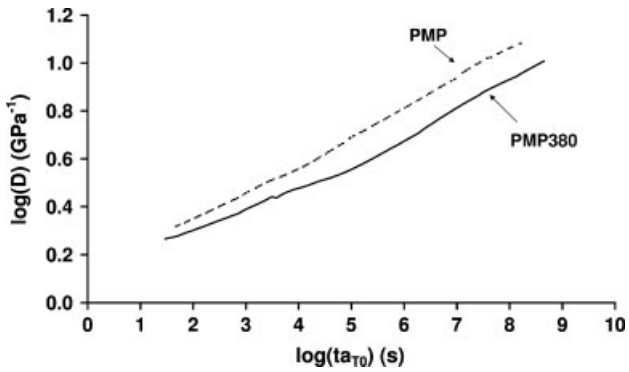

Figure 9. Master curves of PMP (dashed curve) and PMP380 nanocomposite (solid curve) according to a time–temperature superposition principle ($\sigma = 3$ MPa, reference temperature $= 30\,^{\circ}$C).

concerning the isochronous stress–strain curves are consistent with those reported by Yang *et al*. for the creep behaviour of PA66–TiO_2 nanocomposites.[7]

Further information can be obtained by considering the creep compliance curves of Fig. 8, obtained at various temperatures under a given creep stress of 3 MPa. The reduction of the creep compliance of PMP380 is more pronounced at the highest temperature investigated (88 °C). Since the free volume increases as the temperature increases, it is very likely that a temperature rise may influence the creep strain similarly to a stress increase.[31] In order to predict the deformational behaviour for long times, master curves at a reference temperature of 30 °C were constructed, according to a time–temperature superposition principle. The master curves obtained, shown in Fig. 9, clearly show that the creep stability of PMP380 nanocomposites is markedly improved, especially at long loading times. In particular, the master curves indicate that pure PMP reaches a target creep compliance of 10 GPa^{-1} in less than a year, while for PMP380 nanocomposite a time period of more than 12 years is estimated in order to reach the same creep compliance value.

As is evident from Fig. 10, the creep curves of PMP and PMP380 at 30 °C for a constant load of 3 MPa are tentatively fitted by the Findley equation. The parameters resulting from the best fitting of experimental creep data are summarized in Table 4, along with R^2 values. It can be noticed that the Findley model very effectively fits the creep curves, with R^2 values of *ca* 0.99 for all samples. It is evident that the reduction of the creep compliance due to

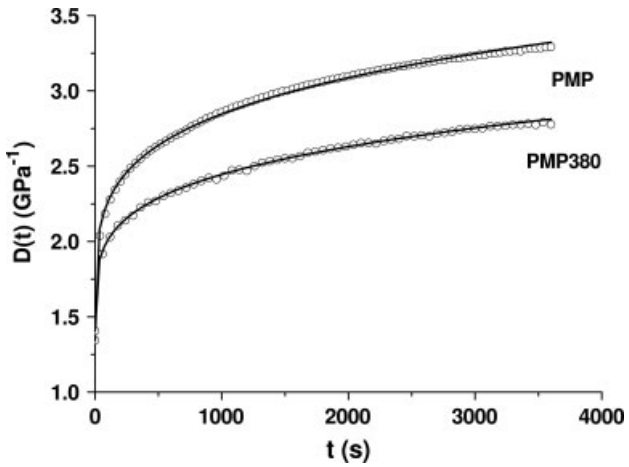

Figure 10. Experimental creep compliance curves (open circles) of PMP and PMP380 samples and theoretical prediction (solid curves) according to the Findley model ($\sigma = 3$ MPa, $T = 30\,^{\circ}$C).

the presence of the silica nanoparticles can be associated with a substantial reduction of the instantaneous creep compliance term D_e and of the coefficient k, related to the retardation relaxation process of the macromolecules, over the entire temperature range. Also, it is worth noting that parameter n is not manifestly affected by the addition of nanoparticles.

Table 4. Fitting parameters of the creep compliance at various temperatures according to the Findley model for PMP and PMP380 ($\sigma = 3$ MPa)

T (°C)	D_e (GPa^{-1})	k (GPa^{-1} s^{-n})	n	R^2
PMP				
30	1.343	0.341	0.215	0.9965
40	2.123	0.365	0.259	0.9977
50	2.278	0.521	0.219	0.9916
65	3.186	0.910	0.223	0.9945
80	3.564	1.430	0.217	0.9874
88	5.073	1.343	0.205	0.9914
PMP380				
30	1.407	0.203	0.237	0.9951
40	2.267	0.272	0.266	0.9984
50	2.463	0.516	0.227	0.9902
65	2.750	0.743	0.231	0.9894
80	3.047	1.199	0.197	0.9705
88	3.250	1.268	0.210	0.9845

CONCLUSIONS

PMP–silica nanocomposites were prepared by melt compounding 2 vol% of fumed silica nanoparticles of various surface areas. The transparency of PMP was substantially maintained for all samples, with no dependence of the optical behaviour on the nanofiller dimensions.

Tensile and dynamic moduli were improved by the presence of the nanoparticles, especially above the glass transition temperature, in particular when high-surface-area nanosilica was used. Creep resistance was considerably improved by the addition of silica, in particular when high stresses and high temperatures were considered. Master curves confirmed the positive effect of silica in increasing the creep stability of PMP. The blocking mechanism of the silica nanoparticles was more effective as the free volume in the material increased, for the effect of temperature or applied stress. Moreover, the silica nanoparticles with the highest surface area were more efficient in reducing the creep compliance of PMP. Fitting of the creep data using Findley's model was effective in modelling the creep behaviour of the samples over the whole range of temperatures considered, parameters D_e and k being substantially reduced by the presence of the nanoparticles.

ACKNOWLEDGEMENT

Ms Nicol Principi is gratefully acknowledged for her support with the experimental work.

REFERENCES

1 Wanjale SD and Jog JP, *Polym Int* **53**:101–105 (2004).
2 Wanjale SD and Jog JP, *J Appl Polym Sci* **90**:3233–3238 (2003).
3 Hadal R, Yuan Q, Jog JP and Misra RDK, *Mater Sci Eng A* **418**:268–281 (2006).
4 Bondioli F, Dorigato A, Fabbri P, Messori M and Pegoretti A, *Polym Eng Sci* **48**:448–457 (2008).
5 Zhang Z, Yang JL and Friedrich K, *Polymer* **45**:3481–3485 (2004).
6 Yang JL, Zhang Z, Schlarb AK and Friedrich K, *Polymer* **47**:6745–6758 (2006).
7 Yang JL, Zhang Z, Schlarb AK and Friedrich K, *Polymer* **47**:2791–2801 (2006).
8 Starkova O, Yang J and Zhang Z, *Compos Sci Technol* **67**:2691–2698 (2007).
9 Siengchin S, Karger-Kocsis J and Thomann R, *J Appl Polym Sci* **105**:2963–2972 (2007).
10 Bondioli F, Dorigato A, Fabbri P, Messori M and Pegoretti A, *J Appl Polym Sci* **112**:1045–1055 (2009).
11 Pegoretti A, Dorigato A and Penati A, *Express Polym Lett* **1**:123–131 (2007).
12 Kontou E and Niaounakis M, *Polymer* **47**:1267–1280 (2006).
13 Ward IM and Hadley DW, *An Introduction to the Mechanical Properties of Solid Polymers*. Wiley, Chichester (1993).
14 Lakes RS, *Viscoelastic Solids*. CRC Press, Boca Raton, FL (1999).
15 Crawford R, *Plastics Engineering*. Pergamon Press, Oxford (1999).
16 Kolarik J, Fambri L, Pegoretti A, Penati A and Goberti P, *Polym Eng Sci* **42**:161–169 (2002).
17 Kolarik J, Pegoretti A, Fambri L and Penati A, *J Appl Polym Sci* **88**:641–651 (2003).
18 Riande E, Calleja RD, Prolongo MG, Masegosa RM and Salom C, *Polymer Viscoelasticity*. Marcel Dekker, New York (2000).
19 Fancey KS, *J Mater Sci* **40**:4827–4831 (2005).
20 Williams G and Watts DC, *Trans Faraday Soc* **66**:80–85 (1970).
21 Palmer RG, Stein DL, Abrahams E and Anderson PW, *Phys Rev Lett* **53**:958–961 (1984).
22 Kohlrausch F, *Poggendorff's Annalen der Physik* **119**:337–368 (1863).
23 Fancey KS, *J Polym Eng* **21**:489–509 (2001).
24 Tomlins PE, *Polymer* **37**:3907–3913 (1996).
25 Findley WN, *Polym Eng Sci* **27**:582–585 (1987).
26 Lietz S, Yang JL, Bosch E, Sandler JKW, Zhang Z and Altstadt V, *Macromol Mater Eng* **292**:23–32 (2007).
27 Ou CF and Hsu MC, *J Polym Res* **14**:373–378 (2007).
28 Ou CF and Hsu MC, *J Appl Polym Sci* **104**:2542–2548 (2007).
29 Zhang MQ, Rong MZ, Zhang HB and Friedrich K, *Polym Eng Sci* **43**:490–500 (2003).
30 Ranade A, Nayak K, Fairbrother D and D'Souzaa NA, *Polymer* **46**:7323–7333 (2005).
31 Kolarik J and Pegoretti A, *Polymer* **47**:346–356 (2006).

